EDGE ARTICLE

Check for updates

Photo-switchable two-dimensional nanofluidic ionic diodes†

Lili Wang,[a] Yaping Feng,[b] Yi Zhou,[c] Meijuan Jia,[b] Guojie Wang,*[a] Wei Guo [ID] *[b] and Lei Jiang[b]

The bottom-up assembly of ion-channel-mimetic nanofluidic devices and materials with two-dimensional (2D) nano-building blocks paves a straightforward way towards the real-world applications of the novel transport phenomena on a nano- or sub-nanoscale. One immediate challenge is to provide the 2D nanofluidic systems with adaptive responsibilities and asymmetric ion transport characteristics. Herein, we introduce a facile and general strategy to provide a graphene-oxide-based 2D nanofluidic system with photo-switchable ionic current rectification (ICR). The degree of ICR can be prominently enhanced upon UV irradiation and it can be perfectly retrieved under irradiation with visible light. A maximum ICR ratio of about 48 was achieved. The smart and functional nanofluidic devices have applications in energy conversion, chemical sensing, water treatment, *etc*.

Introduction

Light-activated ion channels and ion pumps control the electrical properties of biological photoreceptors in a remote and non-invasive way, and play crucial roles in many physiological processes, such as, visual sense, learning, memory, and brain related functions.[1,2] Recent advances in chemistry, materials science, and nanotechnology elicit unprecedented interest in constructing ion-channel-mimetic nanofluidic systems that show adaptive responsiveness to environmental stimuli.[3,4] So far, one dimensional (1D) smart nanofluidic devices in response to pH,[5–7] temperature,[8,9] specific ionic or molecular targets,[10–13] and light irradiation[14,15] have been intensively studied. For example, Wang *et al.* report a photochemical switch in spiropyran modified glass nanopores that selectively transports charged redox species.[16] Taking the advantages of molecular responsiveness in DNA superstructures, we propose a two-way nanopore-based sensing strategy for both oligonucleotides and small-molecule targets with improved signal strength, a lower detection limit, and an anti-interference capability.[17]

The emergence of self-assembled, two-dimensional (2D) material based nanofluidic systems provides a straightforward way to construct 2D yet bulky nanomaterials for real-world applications.[18–23] *Via* the exfoliation–reconstruction strategy, the height of the interstitial lamellar nanochannels is inclined to shrink down to a nano- or sub-nanoscale,[24] comparable with the Debye screening length of the surrounding electrolyte solution, enabling the electrostatic manipulation of the confined ionic species, even at very high ionic strength.[25,26] At the present stage, one great challenge is to endow the 2D nanofluidic systems with adaptive responsibilities and asymmetric ion transport characteristics, creating smart and functionalized nanofluidic devices and materials for practical applications.

Herein, we present photo-switchable 2D nanofluidic diodes that strongly rectify the transmembrane ionic current in response to irradiation with light of different wavelengths. The membrane-scale ionic diode comprises self-assembled graphene oxide (GO) multi-layers, whose capping layers at the uppermost 100–150 nm are decorated with non-covalently attached spiropyran moieties (Fig. 1a). The vertical nanofluidic heterostructure rectifies the ion transport through the membrane. The degree of ionic current rectification (ICR) can be prominently enhanced upon UV irradiation, due to the photochemical conversion of neutral spiropyran to cationic merocyanine, forming charge heterojunctions with the beneath unmodified, negatively charged GO nanochannels. The irradiation of visible light perfectly retrieves the ion transport behavior. A record ICR ratio of about 48 is achieved among existing 2D nanofluidic systems. This asymmetric modification strategy can be generally applied to other kinds of adaptive molecules to create heterostructures in 2D nanofluidic systems, exhibiting diverse responsibilities and asymmetric ion transport characteristics.

[a]Department of Materials Science and Engineering, University of Science and Technology Beijing, Beijing 100083, China. E-mail: guojie.wang@mater.ustb.edu.cn

[b]CAS Key Laboratory of Bio-inspired Materials and Interfacial Science, Technical Institute of Physics and Chemistry, Chinese Academy of Sciences, Beijing 100190, China. E-mail: wguo@iccas.ac.cn

[c]School of Geoscience and Surveying Engineering, China University of Mining and Technology, Beijing 100083, China
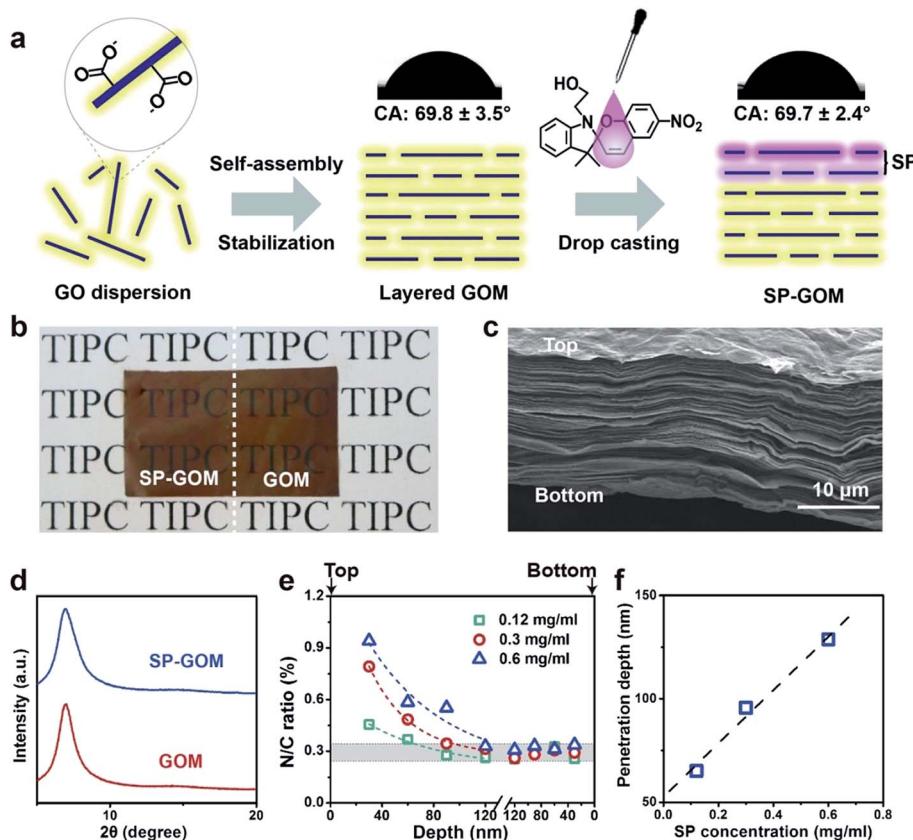
Fig. 1 Spiropyran modified 2D nanofluidic diode membrane. (a) *Via* flow-directed self-assembly and subsequent thermal stabilization, layered graphene oxide membranes (GOMs) with cascading 2D nanochannels were fabricated. A droplet of spiropyran (SP) ethanol solution was dropped on the surface of the GOM from one side. The SP moieties permeate into the top surface layers of the GOM, termed SP-GOM. (b) A photograph of the SP modified (left) and unmodified GOMs (right) placed on a paper substrate with text. The amount of SP is 6 μg cm^{-2}. (c) SEM image on the cross-section of SP-GOM reveals a uniform lamellar structure. (d) XRD patterns of the wet SP-GOM and GOM. The diffraction peaks centered at ~7.0° indicate the interlayer distance of ~1.26 nm. No new ordered structure is found after the SP modification. (e) N/C atomic ratio at different depths beneath the top (left) and bottom (right) surface. From the top surface, the N/C ratio decays with respect to the depth into the GOM, fitted by a natural exponential function (SI). The shadow indicates the background N/C ratio of 0.29 ± 0.05% measured on the GOMs. The deviation is obtained by multiple measurements on different sites. (f) The penetration depth depends on the concentration of SP used for modification.

Results and discussion

Layered graphene oxide membranes (GOMs) were fabricated by flow-directed self-assembly of GO colloids (1.0 mg ml^{-1}).[27] *Via* a mild thermal annealing process,[28] the hydrophilic GOMs can be stabilized in water or in saline for months. The thickness of the GOMs is about 15 μm. 1-(2-Hydroxyethyl)-3, 3-dimethy-lindolino-6′-nitrobenzopyrylospiran (SP) was dissolved in ethanol at a specific concentration. Afterwards, 2 μl of the SP ethanol solution was dropped onto the top surface of the GOM (Fig. 1a). The droplet soon spread on the surface and permeated into the membrane. During the permeation into the GO laminas, the SP moieties attached onto the basal plane of GO through non-covalent interactions, such as π–π interactions, electrostatic interactions, or physical absorption.[29] The SP modified GOM (SP-GOM) is self-supporting, flexible, semi-transparent, and stable in water (Fig. 1b and S1†). Upon hydration, no GO fragments or SP assemblies are found to be re-dissolved in water. The optical appearance, as well as the light transmittance, of the SP-modified and unmodified GOMs are quite similar (Fig. 1b and S2†). The SP-GOM is still hydrophilic on the SP-modified side with a surface contact angle of ~69.7°, which is almost identical to that of unmodified GOMs.

The SP-GOMs exhibit a uniform lamellar microstructure, which can be seen in the cross-sectional view under a scanning electron microscope (Fig. 1c). Similar X-ray diffraction (XRD) peaks centered at ~7.0° indicate an interlayer distance of about 1.26 nm for both the SP-modified and unmodified GOMs in the wet state (Fig. 1d). Grazing incidence X-ray diffraction is also employed to confirm that the single-sided addition of a trace amount of SP does not impair the layered structure of the GOM, even in the near-surface layers (Fig. S3†). Further X-ray photo-electron spectroscopic (XPS) measurements and depth profiling confirm the penetration of the SP moieties into the top surface layers of the GOM. Considering that each SP molecule contains two nitrogen atoms, the attachment of SP on GO promotes the overall nitrogen content. For unmodified GOMs, the back-ground N/C atomic ratio is ~0.29%. After the addition of the SP
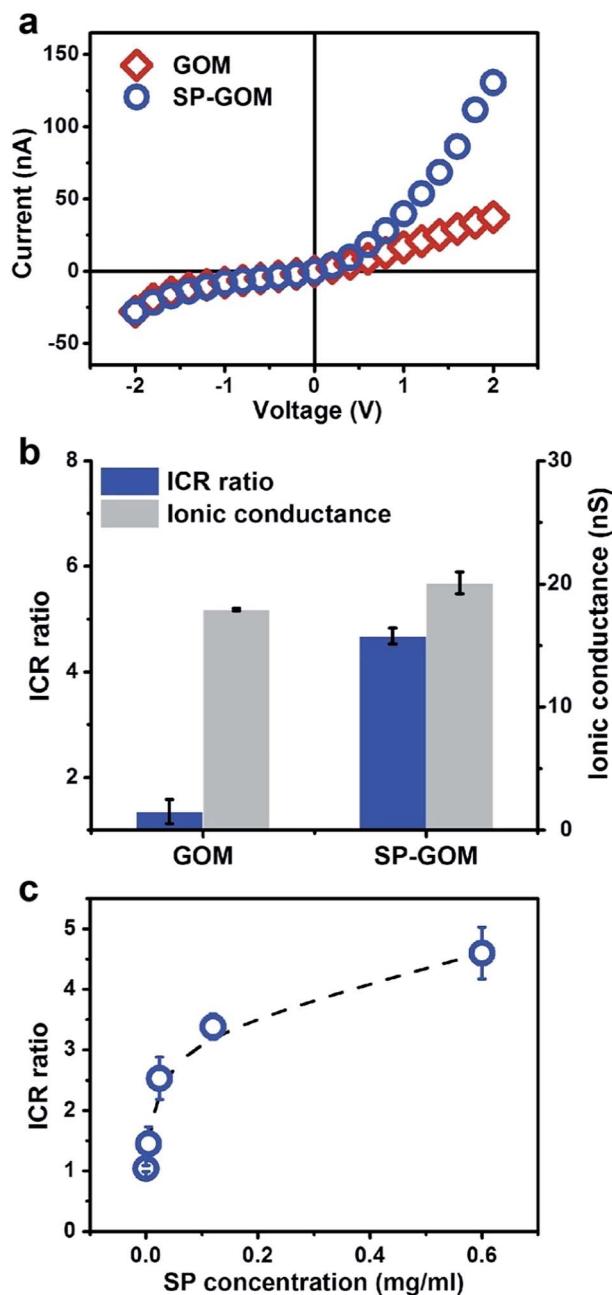
Fig. 2 Rectified ion transport through 2D nanofluidic hetero-structures. (a) Representative current–voltage responses of the SP-modified (circle) and unmodified GOM (square) in 10 mM KCl, pH = 3.0. (b) The ionic current rectification (ICR) ratio and the ionic conductance of the SP-GOM and the GOM are summarized. The asymmetric modification of SP generates rectified transmembrane ion transport, but its influence to the total ionic conductance is very limited. (c) The ICR ratio is controlled by the concentration of SP in the drop-casting process. The concentration of SP for the modification in (a) and (b) is 0.6 mg ml^{-1}.

droplet (0.6 mg ml^{-1}), the N/C atomic ratio increases to about 1.15% on the top surface, and rapidly decays to the level of the unmodified GOM within the uppermost 100–150 nm (Fig. 1e, S4 and S5†). Parallel XPS depth profiling from the bottom of the SP-GOM shows that the nitrogen content there stays at the

background level. The penetration depth of the SP moieties depends on the concentration of SP in the drop-casting process (Fig. 1f). The attached SP molecules do not further penetrate into the membrane after being soaked in water for hours (Fig. S6†).

The formation of the asymmetric membrane structure results in rectified ion transport through the SP-GOM. A piece of the SP-GOM was mounted in a two-compartment photo-electrochemical cell, filled with potassium chloride solution (10 mM, pH = 3.0, Fig. S7†). As typically shown in Fig. 2a, the diode-like current–voltage response is recorded with an ICR ratio of about 4.6. The concentration of SP for the chemical modification is 0.6 mg ml^{-1}. In contrast, the unmodified GOM exhibits a nearly linear ion transport behavior. Besides the asymmetric membrane structure, small amounts of SP moieties may present an open-ring structure in an acidic environment,[30] which also accounts for the observed ICR effect. The asymmetric modification of SP generates rectified ion transport through the entire membrane,[31,32] but it has a very limited influence on the total ionic conductance (Fig. 2b, and S8 and S9†). By increasing the concentration of SP in the drop-casting process, the ICR ratio of the SP-GOMs can be gradually enhanced (Fig. 2c).

Upon UV irradiation (wavelength of 365 nm), the SP-GOM can be excited to a highly rectifying state (Fig. 3a and b). Meanwhile, under the irradiation of visible light (wavelength of 520 nm), the UV-activated ionic current rectification can be perfectly retrieved to the initial state (the resting state) with low rectification. Fig. 3c shows the UV-vis spectra of SP in solution. An absorption maximum at 420-nm is observed after UV irradiation indicating the photoisomerization from the neutral SP state to the cationic merocyanine (MCH$^+$) state.[33] In this process, the spiropyran molecules open the pyran bond and transform to the zwitterionic merocyanine (MC). In acidic solution, the protonation of the phenolate anion yields the cationic MCH$^+$.[30] This transformation can be visualized by the photochromic reaction in an acidic SP solution (Fig. S10 and S11†).[34] Additionally, the GO nanosheets remain negatively charged with a surface potential below −30 mV in acidic solution, down to pH = 3.0 (Fig. S12†). Therefore, the presence of cationic MCH$^+$ contributes positive charges and alters the overall charge density in the surface layers, forming charged heterostructures with the beneath unmodified GO nano-channels (Fig. 3a), that account for the photo-enhanced ionic rectification.[35] Upon the irradiation of visible light, MCH$^+$ can be reversibly converted back to the SP isomer, yielding a fully photo-switchable ionic diode (Fig. S11b†). The photo-induced reversible change in the surface charge properties can also be supported by the zeta potential measurements of the SP modified GO nanosheets (SP-GO) in solution. Upon UV light irradiation, a remarkable positive shift in the zeta potential is found in SP-GO (Fig. S13†), and upon visible light irradiation, the zeta potential drops back to the initial level.

We systematically investigated the time evolution of the current–voltage response of the SP-GOM under UV irradiation. The ICR ratio gradually increases with prolonged illumination time (Fig. 4a). A 58.3% increase in the ICR ratio is found within
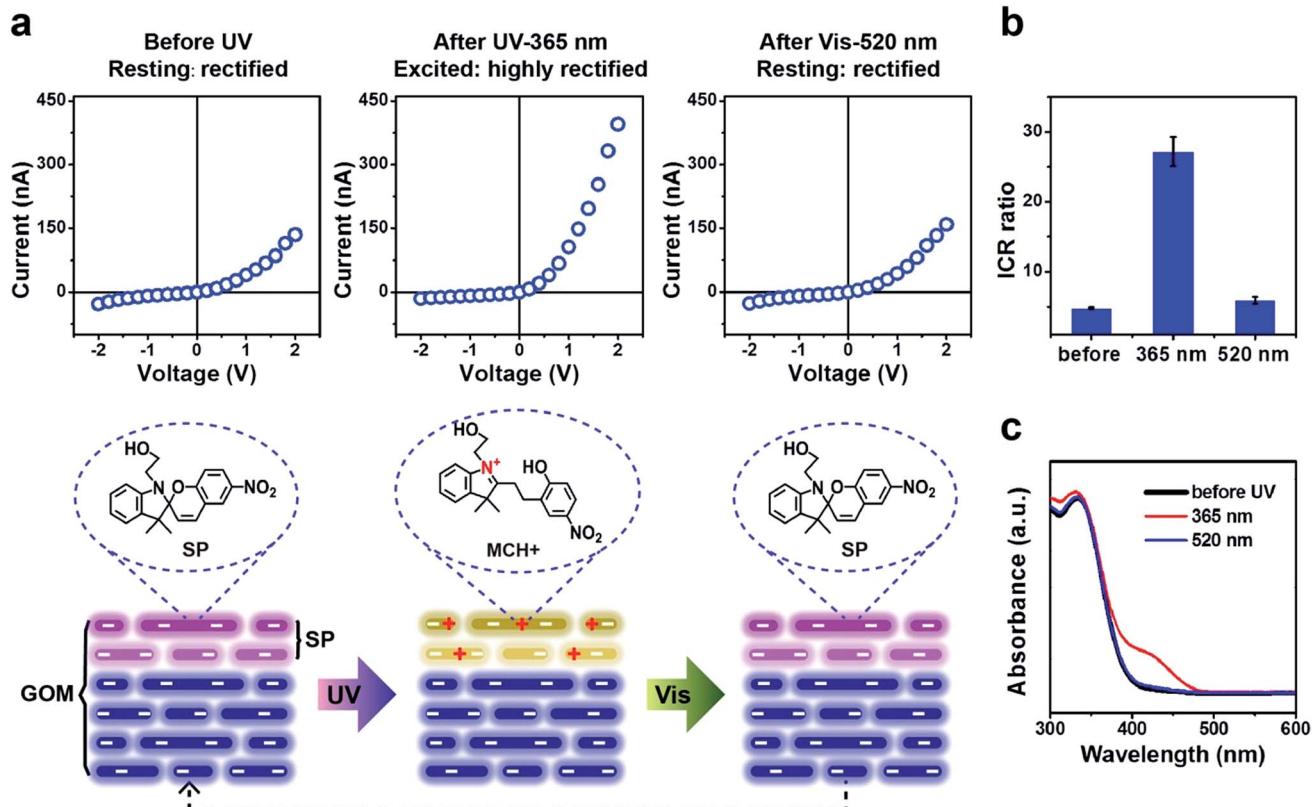
Fig. 3   The photo-switchable 2D nanofluidic diode. (a) Top: current–voltage responses of the SP-GOM before and after irradiation with light of different wavelengths (UV light, 365 nm and visible light, 520 nm). The UV irradiation excites the SP-GOM to a highly rectifying state, and the visible light irradiation perfectly retrieves it to the initial resting state. Bottom: schematic illustration of the photo-induced changes in the molecular and charge state in the multi-layers of the SP-GOM, corresponding to the above current–voltage responses. The ICR ratios are summarized in (b). (c) UV-vis spectra of SP in solution. Upon UV irradiation, an absorption peak at 420 nm is observed (red), indicating the photoisomerization from SP to MCH$^+$. This transformation can be fully retrieved under the irradiation of visible light (blue).

about 5 minutes and a more than 10-fold increment is achieved within 20 minutes. This trend can be supported by the accumulated photoisomerization of the SP molecules in bulk solution. The amount of cationic MCH$^+$ is gradually increased with the duration of UV illumination (Fig. S11a†). A maximum ICR ratio of about 48 is achieved. Although this value is not too high compared to previously reported 1D nanofluidic systems,[36] to the best of our knowledge, it is the best value obtained in existing 2D nanofluidic systems.[37–42] Moreover, the response rate of the SP-GOM is very fast, compared to other responsive nanofluidic systems.[43–45]

The SP-GOM can be reversibly switched between high- and low-rectifying states for many cycles (Fig. 4b). In each cycle, the UV (365 nm) or the visible light (520 nm) irradiation was maintained for 300 seconds. In contrast, the unmodified GOMs stay in a non-rectifying state regardless of the light irradiation. The photo-responsiveness of the SP-GOM is robust. No evident decline in reversibility is found for more than 20 cycles.

Conclusions

In conclusion, for the first time, we integrate light-responsiveness and ionic rectifying functions into a 2D nanofluidic system. The membrane-scale 2D nanofluidic diodes can be reversibly and rapidly switching between high- and low-rectifying states, controlled by light irradiation. The structural and photo-induced charge heterostructures collaboratively result in a prominently enhanced ionic rectification. The maximum ICR ratio of 48 is the best value achieved in existing 2D nanofluidic systems. The bottom-up assembly and asymmetric drop-casting modification provide a facile and general strategy for building smart 2D nanofluidic devices and materials with versatile responsibilities and asymmetric ion transport characteristics for potential applications in energy, environment, sensing, and healthcare related fields.

Experimental section

Membrane fabrication and chemical modification

The GOMs were prepared by the vacuum filtration of 40 ml of a GO dispersion (1.0 mg ml^{-1}) through a mixed cellulose ester membrane (47 mm in diameter, effective pore size of 0.1 μm). To stabilize the hydrophilic GOMs, they were heated at 80 °C for 24 hours in an oven before use. 6.0 mg of 1-(2-hydroxyethyl)-3, 3-dimethylindolino-6′-nitrobenzopyrylospiran (SP) was dissolved in 10 ml of ethanol. To obtain the SP-GOM, a droplet of SP
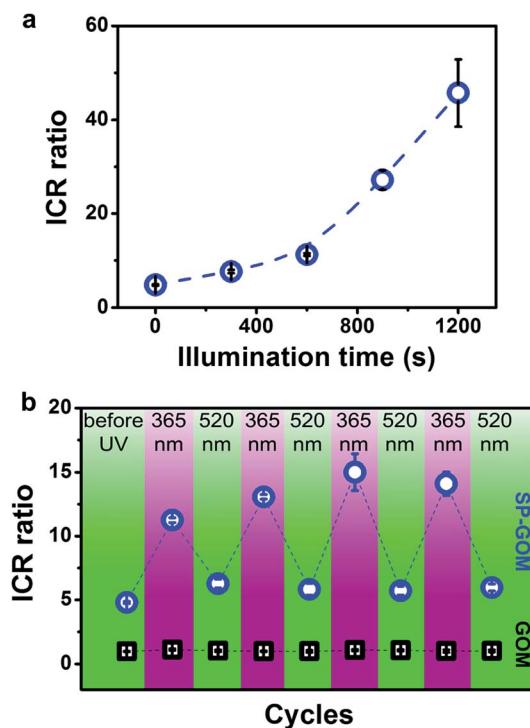
Fig. 4 Time evolution and reversibility. (a) The rectification ratio of the SP-GOM gradually enhances with prolonged illumination time. (b) Repeated cycles under alternating UV and visible light irradiation. The SP-GOMs show excellent reversibility in the ionic rectifying properties controlled by light. In contrast, the unmodified GOMs are insensitive to light irradiation showing non-rectified ion transport behavior. The concentration of SP for chemical modification is 0.6 mg ml^{-1}.

ethanol solution (2 μl) was dropped onto the top surface of the GOM. Afterwards, the samples were dried in air at room temperature for about 30 minutes.

Characterization

The surface charge property of the GO colloids (1.0 mg ml^{-1}) was measured by zeta potential on a Malvern Zetasizer NanoZS90. The surface contact angle was measured using an OCA20 contact-angle system (Data Physics, Germany) at room temperature. The microstructures of the GOM and SP-GOM were characterized by a scanning electronic microscope (SEM, Hitachi S4800). X-ray diffraction (XRD) characterization was carried out using a polycrystalline X-ray diffractometer with a Cu radiation source (Bruker D8 Advance). X-ray photoelectron spectroscopy (XPS) tests were performed on an ESCALAB250Xi electron spectrometer from TF Scientific, using 300 W Al Kα radiations.[46] Depth profiling was conducted by the Ar-ion etching of the SP-GOM to a determined depth, for collecting spectra. The UV-vis absorption spectrum was obtained on a JASCO V-570 spectrophotometer.

Electrical measurements

The testing membrane was mounted in between the two chambers of a custom-designed electrochemical cell, with one side open to the light source through a glass seal (Fig. S7†).[47,48] The light source was two 500 W high-pressure mercury lamps, providing UV (365 nm) and visible (520 nm) light irradiation, separately. The light intensity was 25 mW cm^{-2}. The two light sources were held at the same distance from the samples. The effective membrane area for the current recording is 1.6 mm^2. The transmembrane ionic current was recorded by a source meter (Keithley 2636B) with Ag/AgCl electrodes. During the light irradiation, no electrodes were placed in the electrochemical cell to avoid light pollution. A 10 mM KCl solution was used as the electrolyte. The ionic conductance was measured at a low voltage range within ± 100 mV. The ICR ratio was measured at a high voltage of ±2.0 V.

Acknowledgements

References

1 M. Banghart, K. Borges, E. Isacoff, D. Trauner and R. H. Kramer, *Nat. Neurosci.*, 2004, **7**, 1381–1386.
2 M. R. Banghart, M. Volgraf and D. Trauner, *Biochemistry*, 2006, **45**, 15129–15141.
3 Z. S. Siwy and S. Howorka, *Chem. Soc. Rev.*, 2010, **39**, 1115–1132.
4 W. Guo, Y. Tian and L. Jiang, *Acc. Chem. Res.*, 2013, **46**, 2834–2846.
5 R. Casasús, E. Climent, M. D. Marcos, R. Martínez-Máñez, F. Sancenón, J. Soto, P. Amorós, J. Cano and E. Ruiz, *J. Am. Chem. Soc.*, 2008, **130**, 1903–1917.
6 B. Yameen, M. Ali, R. Neumann, W. Ensinger, W. Knoll and O. Azzaroni, *J. Am. Chem. Soc.*, 2009, **131**, 2070–2071.
7 S. F. Buchsbaum, G. Nguyen, S. Howorka and Z. S. Siwy, *J. Am. Chem. Soc.*, 2014, **136**, 9902–9905.
8 B. Yameen, M. Ali, R. Neumann, W. Ensinger, W. Knoll and O. Azzaroni, *Small*, 2009, **5**, 1287–1291.
9 W. Guo, H. Xia, F. Xia, X. Hou, L. Cao, L. Wang, J. Xue, G. Zhang, Y. Song, D. Zhu, Y. Wang and L. Jiang, *ChemPhysChem*, 2010, **11**, 859–864.
10 L. Cao, W. Guo, W. Ma, L. Wang, F. Xia, S. Wang, Y. Wang, L. Jiang and D. Zhu, *Energy Environ. Sci.*, 2011, **4**, 2259–2266.
11 M. Ali, S. Nasir, Q. H. Nguyen, J. K. Sahoo, M. N. Tahir, W. Tremel and W. Ensinger, *J. Am. Chem. Soc.*, 2011, **133**, 17307–17314.
12 S. W. Kowalczyk, L. Kapinos, T. R. Blosser, T. Magalhaes, P. van Nies, Y. H. LimRoderick and C. Dekker, *Nat. Nanotechnol.*, 2011, **6**, 433–438.
13 Y. Jiang, N. Liu, W. Guo, F. Xia and L. Jiang, *J. Am. Chem. Soc.*, 2012, **134**, 15395–15401.

14 I. Vlassiouk, C. D. Park, S. A. Vail, D. Gust and S. Smirnov, *Nano Lett.*, 2006, **6**, 1013–1017.

15 X. Zhang, J. Zhang, Y.-L. Ying, H. Tian and Y.-T. Long, *Chem. Sci.*, 2014, **5**, 2642–2646.

16 G. Wang, A. K. Bohaty, I. Zharov and H. S. White, *J. Am. Chem. Soc.*, 2006, **128**, 13553–13558.

17 N. Liu, Y. Jiang, Y. Zhou, F. Xia, W. Guo and L. Jiang, *Angew. Chem., Int. Ed.*, 2013, **52**, 2007–2011.

18 A. R. Koltonow and J. Huang, *Science*, 2016, **351**, 1395–1396.

19 W. Guo and L. Jiang, *Sci. China Mater.*, 2014, **57**, 2–6.

20 G. Liu, W. Jin and N. Xu, *Angew. Chem., Int. Ed.*, 2016, **55**, 13384–13397.

21 Z. Zheng, R. Grunker and X. Feng, *Adv. Mater.*, 2016, **28**, 6529–6545.

22 J. Gao, W. Guo, H. Geng, X. Hou, Z. Shuai and L. Jiang, *Nano Res.*, 2012, **5**, 99–108.

23 L. Lin, L. Zhang, L. Wang and J. Li, *Chem. Sci.*, 2016, **7**, 3645–3648.

24 X. Yang, C. Cheng, Y. Wang, L. Qiu and D. Li, *Science*, 2013, **341**, 534–537.

25 H. G. Park and Y. Jung, *Chem. Soc. Rev.*, 2014, **43**, 565–576.

26 P. Z. Sun, K. L. Wang and H. W. Zhu, *Adv. Mater.*, 2016, **28**, 2287–2310.

27 C. Cheng and D. Li, *Adv. Mater.*, 2013, **25**, 13–30.

28 J. Ji, Q. Kang, Y. Zhou, Y. Feng, X. Chen, J. Yuan, W. Guo, Y. Wei and L. Jiang, *Adv. Funct. Mater.*, 2017, **27**, 1603623.

29 X. Zhang, L. Hou and P. Samori, *Nat. Commun.*, 2016, **7**, 11118.

30 R. Klajn, *Chem. Soc. Rev.*, 2014, **43**, 148–184.

31 Y. Green, Y. Edri and G. Yossifon, *Phys. Rev. E*, 2015, **92**, 033018.

32 L. Cao, F. Xiao, Y. Feng, W. Zhu, W. Geng, J. Yang, X. Zhang, N. Li, W. Guo and L. Jiang, *Adv. Funct. Mater.*, 2017, **27**, 1604302.

33 C. Liu, D. Yang, Q. Jin, L. Zhang and M. Liu, *Adv. Mater.*, 2016, **28**, 1644–1649.

34 H. Komber, S. Müllers, F. Lombeck, A. Held, M. Walter and M. Sommer, *Polym. Chem.*, 2014, **5**, 443–453.

35 L. J. Cheng and L. J. Guo, *Chem. Soc. Rev.*, 2010, **39**, 923–938.

36 J. Gao, W. Guo, D. Feng, H. Wang, D. Zhao and L. Jiang, *J. Am. Chem. Soc.*, 2014, **136**, 12265–12272.

37 K. Raidongia and J. X. Huang, *J. Am. Chem. Soc.*, 2012, **134**, 16528–16531.

38 P. Sun, M. Zhu, K. Wang, M. Zhong, J. Wei, D. Wu, Z. Xu and H. Zhu, *ACS Nano*, 2013, **7**, 428–437.

39 W. Guo, C. Cheng, Y. Wu, Y. Jiang, J. Gao, D. Li and L. Jiang, *Adv. Mater.*, 2013, **25**, 6064–6068.

40 R. K. Joshi, P. Carbone, F. C. Wang, V. G. Kravets, Y. Su, I. V. Grigorieva, H. A. Wu, A. K. Geim and R. R. Nair, *Science*, 2014, **343**, 752–754.

41 M. Miansari, J. R. Friend and L. Y. Yeo, *Adv. Sci.*, 2015, **2**, 1500062.

42 Y. Jiang, J. Gao, W. Guo and L. Jiang, *Chem. Commun.*, 2014, **50**, 14149–14152.

43 F. Xia, W. Guo, Y. Mao, X. Hou, J. Xue, H. Xia, L. Wang, Y. Song, H. Ji, Q. Ouyang, Y. Wang and L. Jiang, *J. Am. Chem. Soc.*, 2008, **130**, 8345–8350.

44 W. Guo, H. Xia, L. Cao, F. Xia, S. Wang, G. Zhang, Y. Song, Y. Wang, L. Jiang and D. Zhu, *Adv. Funct. Mater.*, 2010, **20**, 3561–3567.

45 W. Guo, F. Hong, N. N. Liu, J. Y. Huang, B. Y. Wang, R. X. Duan, X. D. Lou and F. Xia, *Adv. Mater.*, 2015, **27**, 2090–2095.

46 C. N. Yeh, K. Raidongia, J. Shao, Q. H. Yang and J. Huang, *Nat. Chem.*, 2014, **7**, 166–170.

47 W. Guo, L. X. Cao, J. C. Xia, F. Q. Nie, W. Ma, J. M. Xue, Y. L. Song, D. B. Zhu, Y. G. Wang and L. Jiang, *Adv. Funct. Mater.*, 2010, **20**, 1339–1344.

48 L. Cao, W. Guo, Y. Wang and L. Jiang, *Langmuir*, 2012, **28**, 2194–2199.